

Temperature dependence of the symmetry energy and neutron skins in Ni, Sn, and Pb isotopic chains

A. N. Antonov,¹ D. N. Kadrev,¹ M. K. Gaidarov,¹ P. Sarriguren,² and E. Moya de Guerra³

¹*Institute for Nuclear Research and Nuclear Energy, Bulgarian Academy of Sciences, Sofia 1784, Bulgaria*

²*Instituto de Estructura de la Materia, IEM-CSIC, Serrano 123, E-28006 Madrid, Spain*

³*Grupo de Física Nuclear, Departamento de Física Atómica, Molecular y Nuclear, Facultad de Ciencias Físicas, Universidad Complutense de Madrid, E-28040 Madrid, Spain*

(Received 29 September 2016; published 14 February 2017; publisher error corrected 28 February 2017)

The temperature dependence of the symmetry energy for isotopic chains of even-even Ni, Sn, and Pb nuclei is investigated in the framework of the local density approximation (LDA). The Skyrme energy density functional with two Skyrme-class effective interactions, SkM* and SLy4, is used in the calculations. The temperature-dependent proton and neutron densities are calculated through the HFBTHO code that solves the nuclear Skyrme-Hartree-Fock-Bogoliubov problem by using the cylindrical transformed deformed harmonic-oscillator basis. In addition, two other density distributions of ²⁰⁸Pb, namely the Fermi-type density determined within the extended Thomas-Fermi (TF) method and symmetrized-Fermi local density obtained within the rigorous density functional approach, are used. The kinetic energy densities are calculated either by the HFBTHO code or, for a comparison, by the extended TF method up to second order in temperature (with T^2 term). Alternative ways to calculate the symmetry energy coefficient within the LDA are proposed. The results for the thermal evolution of the symmetry energy coefficient in the interval $T = 0\text{--}4$ MeV show that its values decrease with temperature. The temperature dependence of the neutron and proton root-mean-square radii and corresponding neutron skin thickness is also investigated, showing that the effect of temperature leads mainly to a substantial increase of the neutron radii and skins, especially in the more neutron-rich nuclei, a feature that may have consequences on astrophysical processes and neutron stars.

DOI: [10.1103/PhysRevC.95.024314](https://doi.org/10.1103/PhysRevC.95.024314)

I. INTRODUCTION

In recent years, many studies have been carried out to understand the density dependence of the nuclear equation of state (EOS) over a wide range of densities and temperatures (see, e.g., Ref. [1,2] and the topical issue of the European Physical Journal A on nuclear symmetry energy (NSE) [3]). This is needed for a reliable treatment of a large variety of nuclear and astrophysical phenomena. One very important ingredient of the EOS from both experimental and theoretical aspects is the symmetry energy that describes the dependence of the energy per nucleon on the proton-to-neutron ratio. It is important to distinguish between finite nuclei and infinite nuclear matter, where, for the latter, the Coulomb interaction is turned off. Nuclear matter is characterized by its energy per particle as a function of density and other thermodynamic quantities (e.g., temperature). At the same time, within, e.g., the local-density approximation (LDA) [4–7] or coherent density fluctuation model (CDFM) [8–10], one can use the EOS of asymmetric nuclear matter (ANM) to obtain information on finite systems.

The nuclear symmetry energy, as a fundamental quantity in nuclear physics and astrophysics, represents a measure of the energy gain in converting isospin asymmetric nuclear matter to a symmetric system. Its value depends on the density ρ and temperature T . Experimentally, the nuclear symmetry energy is not a directly measurable quantity and is extracted indirectly from observables that are related to it (e.g., [11,12]). The need for information on the symmetry energy in finite nuclei (including the one theoretically obtained) is a major issue because it allows one to constrain the bulk and surface properties of the nuclear energy-density functionals (EDFs) quite effectively. More information on the nuclear symmetry

energy is still required for understanding the structures of nuclei far away from the β -stability line, heavy-ion collisions, supernova explosions, and neutron star properties. As can be seen, e.g., in Refs. [13–17], an increasingly wide range of theoretical ideas are being proposed on the density dependence of the symmetry energy as well as on some associated nuclear characteristics. In recent years, the temperature dependence of single-particle properties in nuclear and neutron matter was also broadly investigated, including studies in finite systems, as well (e.g., Refs. [4,18–25]).

The thermal behavior of the symmetry energy has a role in changing the location of the nuclear drip lines as nuclei warm up. Also, it is of fundamental importance for the liquid-gas phase transition of asymmetric nuclear matter, the dynamical evolution mechanisms of massive stars and the supernova explosion [26]. Since the density derivative of the symmetry coefficient reflects the pressure difference on the neutrons and protons and is thus one of the determinants in fixing the neutron skin of nuclei, the nature and stability of phases within a warm neutron star, its crustal composition, or its crust thickness [27] would be strongly influenced by the temperature dependence of the symmetry energy.

The problem of accurate treatment of the thermodynamical properties of hot finite nuclei is still challenging. Since the pioneering work of Brack and Quentin [28] on thermal Hartree-Fock (HF) calculations, various methods have been developed to study the dynamical evolution of such excited systems. Among them we note semiclassical approaches based on the microscopic Skyrme-HF formalism [29] and Thomas-Fermi (TF) approximation [30] with inclusion of the continuum effects in HF calculations at finite temperature [31].

Further, a refined Thomas-Fermi description of hot nuclei was reported in Ref. [32]. The extended Thomas-Fermi (ETF) model proposed by Brack in Ref. [33] through inclusion of second-order gradient corrections to the TF density functionals showed their decisive role in obtaining an excellent agreement with HF results. More recently, Hartree-Fock-Bogoliubov (HFB) models [34–36] and a finite-temperature HF+BCS approximation with zero-range Skyrme forces [37] have been developed. A relativistic TF approximation with different relativistic mean-field (RMF) nuclear interactions has been also explored to extract the symmetry energy coefficient for several representative nuclei and to study its temperature dependence [21].

A sensitive probe of the nuclear symmetry energy is the neutron-skin thickness of nuclei (see, for example, Ref. [38] and references therein). The latter is commonly defined in terms of the difference between the neutron and proton root-mean-square (rms) radii and is found to be closely related to the density dependence of the NSE, with the EOS of pure neutron matter and properties of neutron stars [39–46]. It is also related to a number of observables in finite nuclei, including the NSE (see, e.g., [4,8,9,47–65]), although its precise measurement is difficult. As examples, in Ref. [37] Yüksel *et al.* analyzed the temperature dependence of the nuclear radii for the ^{120}Sn nucleus and neutron skin as a function of N/Z value for the tin isotopic chain within the finite-temperature HF+BCS framework using Skyrme interactions. The same nuclear characteristics were computed within the relativistic TF approximation for ^{56}Fe and ^{208}Pb nuclei in Ref. [21], where both neutron and proton rms radii were found to increase significantly with increasing T , comparable to those shown in Ref. [30] from HF calculations.

In our previous works [8,9] the symmetry energy was studied in a wide range of spherical and deformed nuclei on the basis, as an example, of the Brueckner EDF of ANM [66,67]. In these works the transition from the properties of nuclear matter to those of finite nuclei was made using the coherent density fluctuation model [68,69]. In Ref. [8] a study of the correlation between the thickness of the neutron skin in finite nuclei and the nuclear symmetry energy (s) for the isotopic chains of even-even Ni ($A = 74\text{--}84$), Sn ($A = 124\text{--}152$) and Pb ($A = 206\text{--}214$) nuclei, also the neutron pressure (p_0) and the asymmetric compressibility (ΔK) for these nuclei was performed. The calculations were based on the deformed self-consistent mean-field HF+BCS method using the CDFM and the Brueckner EDF. The same approaches were used in Ref. [9] for the calculations of the mentioned quantities of deformed neutron-rich even-even nuclei, such as Kr ($A = 82\text{--}120$) and Sm ($A = 140\text{--}156$) isotopes. The numerical results for s , p_0 , and ΔK for neutron-rich and neutron-deficient Mg isotopes with $A = 20\text{--}36$ were presented in Ref. [10].

The main aim of this work is, apart from the ρ dependence investigated in our previous works [8–10], to study also the temperature dependence of the symmetry energy in finite nuclei. We focus on the determination of the symmetry energy coefficient, for which we have explored the local density approximation [4–7] with some modifications. In the present paper the thermal evolution of the symmetry energy coefficient

is investigated for Ni, Sn, and Pb isotopic chains in the interval $T = 0\text{--}4$ MeV using different model temperature-dependent local density distributions for these nuclei. We restrict ourselves to this temperature range because, in accordance with several findings (e.g., in Ref. [70]), the limiting temperature (above which the nucleus cannot exist as a bound system) has been evaluated to be around 4 MeV for finite nuclei with mass number $A \geq 100$. The temperature-dependent densities of these nuclei are calculated within a self-consistent Skyrme-HFB method using the cylindrical transformed deformed harmonic-oscillator basis (HFBTHO densities) [71,72]. The kinetic energy density is calculated either by the HFBTHO code or by the TF expression up to T^2 term [22]. We have used two parametrizations of the Skyrme force, namely, SLy4 and SkM*, which were able to give an appropriate description of bulk properties of spherical and deformed nuclei in the past. In addition, we present some results for the ^{208}Pb nucleus with densities obtained within the ETF method [29,33] and the rigorous density functional approach (RDFA) [73]. The effect of temperature on the rms radii of protons and neutrons and the formation of neutron skin in hot nuclei is also analyzed and discussed.

This article is organized as follows. In Sec. II, we give the theoretical elements to obtain the symmetry energy coefficient and briefly describe the temperature-dependent nuclear densities. In Sec. III, we present the numerical results for hot nuclei properties and the temperature dependence of the symmetry energy of finite nuclei. Section IV contains the conclusions.

II. THEORETICAL FORMALISM

A. Temperature-dependent symmetry energy coefficient with Skyrme energy density functional

For finite systems, different definitions of the symmetry energy coefficient and its temperature dependence are considered in the literature. In the present paper we develop an approach to calculate the symmetry energy coefficient for a specific nucleus starting with the LDA expression given in [4,5]:

$$e_{\text{sym}}(A, T) = \frac{1}{I^2 A} \int \rho(r) e_{\text{sym}}[\rho(r), T] \delta^2(r) d^3r. \quad (1)$$

In Eq. (1) $I = (N - Z)/A$, $e_{\text{sym}}[\rho(r), T]$ is the symmetry energy coefficient at temperature T of infinite nuclear matter at the value of the total local density $\rho(r) = \rho_n(r) + \rho_p(r)$, $\delta(r) = [\rho_n(r) - \rho_p(r)]/\rho(r)$ is the ratio between the isovector and the isoscalar parts of $\rho(r)$, with $\rho_n(r)$ and $\rho_p(r)$ being the neutron and proton local densities. The symmetry energy coefficient $e_{\text{sym}}(\rho, T)$ can be evaluated in different ways. Following Refs. [4,7], we adopt in this work the definition

$$e_{\text{sym}}(\rho, T) = \frac{e(\rho, \delta, T) - e(\rho, \delta = 0, T)}{\delta^2}, \quad (2)$$

where $e(\rho, \delta, T)$ is the energy per nucleon in an asymmetric infinite matter, while $e(\rho, \delta = 0, T)$ is that one of symmetric nuclear matter. These quantities are expressed by $e = \mathcal{E}(r, T)/\rho$, where $\mathcal{E}(r, T)$ is the total energy density of the

system. For the Skyrme energy density functional that we use in our work it has the form

$$\begin{aligned} \mathcal{E}(r, T) = & \frac{\hbar^2}{2m_{n,k}} \tau_n + \frac{\hbar^2}{2m_{p,k}} \tau_p \\ & + \frac{1}{2} t_0 \left[\left(1 + \frac{1}{2} x_0 \right) \rho^2 - \left(x_0 + \frac{1}{2} \right) (\rho_n^2 + \rho_p^2) \right] \\ & + \frac{1}{12} t_3 \rho^\alpha \left[\left(1 + \frac{x_3}{2} \right) \rho^2 - \left(x_3 + \frac{1}{2} \right) (\rho_n^2 + \rho_p^2) \right] \\ & + \frac{1}{16} \left[3t_1 \left(1 + \frac{1}{2} x_1 \right) - t_2 \left(1 + \frac{1}{2} x_2 \right) \right] (\nabla \rho)^2 \\ & - \frac{1}{16} \left[3t_1 \left(x_1 + \frac{1}{2} \right) + t_2 \left(x_2 + \frac{1}{2} \right) \right] \\ & \times [(\nabla \rho_n)^2 + (\nabla \rho_p)^2] + \mathcal{E}_c(r), \end{aligned} \quad (3)$$

where for infinite homogeneous nuclear matter only the first three lines of Eq. (3) contribute. The derivative terms vanish and the Coulomb term \mathcal{E}_c is neglected. In Eq. (3) $t_0, t_1, t_2, t_3, x_0, x_1, x_2, x_3$, and α are the Skyrme parameters. We use in this work the interactions SkM* [74] and SLy4 [75]. The nucleon effective mass $m_{q,k}$ is defined through

$$\begin{aligned} \frac{m}{m_{q,k}(r)} = & 1 + \frac{m}{2\hbar^2} \left\{ \left[t_1 \left(1 + \frac{x_1}{2} \right) + t_2 \left(1 + \frac{x_2}{2} \right) \right] \rho \right. \\ & \left. + \left[t_2 \left(x_2 + \frac{1}{2} \right) - t_1 \left(x_1 + \frac{1}{2} \right) \right] \rho_q \right\}, \end{aligned} \quad (4)$$

with $q = (n, p)$ referring to neutrons or protons. The dependence on temperature of $\mathcal{E}(r, T)$ [Eq. (3)] and $m/m_{q,k}(r)$ [Eq. (4)] comes from the T dependence of the densities and kinetic energy densities.

A self-consistent approach based on the simultaneous treatment of temperature-dependent density distributions and kinetic energy density is related to the finite-temperature formalism for the HFB method. In it the nuclear Skyrme-HFB problem is solved by using the transformed harmonic-oscillator basis [71]. The HFBTHO code based on the mentioned approach is used in our numerical calculations.

The HFBTHO code solves the finite-temperature HFB equations assuming axial and time-reversal symmetry. These equations are formally equivalent to the HFB equations at $T = 0$ if the expressions of the density matrix ρ and pairing tensor κ are redefined as

$$\begin{aligned} \rho &= U f U^\dagger + V^* (1 - f) V^T, \\ \kappa &= U f V^\dagger + V^* (1 - f) U^T, \end{aligned} \quad (5)$$

where U and V are the matrices of the Bogoliubov transformation (here T means transpose) and f is the temperature-dependent Fermi-Dirac factor given by

$$f_i = (1 + e^{E_i/k_B T})^{-1}. \quad (6)$$

In this expression E_i is the quasiparticle energy of the state i and k_B is the Boltzmann constant. In HFBTHO the Fermi level λ is determined at each iteration from the conservation

of particle number in BCS approach [71],

$$N(\lambda) = \sum_i [v_i(\lambda)^2 + f_i(\lambda)(u_i(\lambda)^2 - v_i(\lambda)^2)], \quad (7)$$

where the BCS occupations are given by

$$v_i^2 = \frac{1}{2} \left[1 - \frac{e_i - \lambda}{E_i^{BCS}} \right], \quad u_i^2 = 1 - v_i^2, \quad (8)$$

and $E_i^{BCS} = [(e_i - \lambda)^2 + \Delta_i^2]^{1/2}$. Note that at $T = 0$ the Fermi-Dirac factors are zero and one recovers the usual expressions for ρ and κ in Eq. (5) and for the number of particles in Eq. (7).

B. Temperature-dependent kinetic energy density

There exist various methods to obtain the kinetic energy density $\tau_q(r, T)$ entering the expression for $\mathcal{E}(r, T)$ [Eq. (3)]. One of them is, as mentioned above, to use the HFBTHO code. Another way is to use the TF approximation adopted in Ref. [4], or an extension of the TF expression up to T^2 terms [22]:

$$\begin{aligned} \tau_q(r, T) = & \frac{2m}{\hbar^2} \varepsilon_{K_q} = \frac{3}{5} (3\pi^2)^{2/3} \\ & \times \left[\rho_q^{5/3} + \frac{5\pi^2 m_q^2}{3\hbar^4} \frac{1}{(3\pi^2)^{4/3}} \rho_q^{1/3} T^2 \right]. \end{aligned} \quad (9)$$

In Eq. (9) the first term in square brackets is the degenerate limit at zero temperature and the T^2 term is the finite-temperature correction. By using the approximate expression (9) for the kinetic energy density, Lee and Mekjian performed calculations of the volume and surface symmetry energy coefficients for finite nuclei in Ref. [22], showing that the surface symmetry energy term is the most sensitive to the temperature while the bulk energy term is the least sensitive. In the present work we calculate the kinetic energy density using the self-consistent Skyrme-HFB method and the HFBTHO code. Also, for a comparison we present the results when using $\tau_q(r, T)$ from Eq. (9).

C. Temperature-dependent densities

In our work the local density distributions are calculated by the HFBTHO code [71]. The T -dependent proton and neutron densities $\rho_q(\vec{r}, T)$ normalized by

$$\int \rho_q(\vec{r}, T) d\vec{r} = Q, \quad Q = Z, N \quad (10)$$

determine the corresponding mean square radii

$$\langle R_q^2 \rangle = \frac{\int r^2 \rho_q(\vec{r}, T) d\vec{r}}{\int \rho_q(\vec{r}, T) d\vec{r}}, \quad (11)$$

the rms radii

$$R_q = \langle R_q^2 \rangle^{1/2}, \quad (12)$$

and the neutron skin thickness which is usually characterized by the difference of the neutron and proton rms radii:

$$\Delta R = R_n - R_p. \quad (13)$$

In addition, two other density distributions of ^{208}Pb [76], namely the Fermi-type density determined within the ETF method [29,33] and the symmetrized-Fermi local density obtained within the rigorous density functional approach (RDFA) [73], are used. The density within the ETF method [29,33], which is the semi-classical limit of the temperature-dependent Hartree-Fock (THF) theory [28], has the form

$$\rho_{ETF}(r, T) = \rho_0(T) \left\{ 1 + \exp \left[\frac{r - R(T)}{\alpha(T)} \right] \right\}^{-\gamma(T)}. \quad (14)$$

The temperature-dependent local density parameters ρ_0 , R , α , and γ are obtained for the nucleus ^{208}Pb with the SkM* effective force. The local densities (14) reproduce the averaged THF results up to temperature $T = 4$ MeV [28]. The symmetrized-Fermi local density distribution determined for the same nucleus within the RDFA [73] is

$$\rho_{SF}(r, T) = \rho_0(T) \frac{\sinh[R(T)/b(T)]}{\cosh[R(T)/b(T)] + \cosh[r/b(T)]}. \quad (15)$$

The temperature-dependent local density parameters ρ_0 , R , and b are obtained with the SkM effective force up to $T = 10$ MeV. As demonstrated in [73], the RDFA reproduces almost exactly the THF results [31] up to temperatures $T = 8$ MeV above which the nucleus is unstable with respect to the THF calculations [31].

D. Relationships for calculations of T -dependent symmetry energy coefficient

As mentioned in Sec. II A, in the present work we use the approach given by Eqs. (1) and (2), as well as the T -dependent Skyrme EDF [Eq. (3)] to calculate the symmetry energy coefficient. Here we note the specific problem that arises, namely how to calculate the term $e(\rho, \delta = 0, T)$ of Eq. (2) that is responsible for the contribution of the energy per particle of symmetric nuclear matter. One of the expressions shown in Ref. [7] to calculate $e_{\text{sym}}(T)$ for a nucleus with mass number A is in the spirit of the liquid-drop model, and has the form

$$e_{\text{sym}}(T) = [e(N, Z, T) - e(A/2, A/2, T)]/X^2, \quad (16)$$

where $X = (N - Z)/A$ is the asymmetry parameter. Eq. (16) is valid when the energy per particle of the nucleus e does not contain the Coulomb contribution. As pointed out in Ref. [7] in the cases of relatively heavy nuclei, the stable systems are usually isospin-asymmetric and then, the definition given by Eq. (16) may not be operative. The suggested expression in [4,7] is

$$e_{\text{sym}}(T) = [e(A, X_1, T) - e(A, X_2, T)]/(X_1^2 - X_2^2), \quad (17)$$

where X_1 and X_2 are the asymmetry parameters of the nuclear pair. As concluded in [7], the value of $e_{\text{sym}}(T)$ from Eqs. (16) and (17) depends on the choice of the nuclear pair and, thus, its value is not unambiguous for a particular nucleus.

Therefore, in our study aiming to investigate the temperature dependence of e_{sym} within a given isotopic chain, we introduce other definitions of $e_{\text{sym}}(A, T)$ in the LDA that, in our opinion, would be more appropriate in this case. They concern namely the above mentioned problem of calculating the term $e(\rho, \delta = 0, T)$ of Eq. (2) for symmetric nuclear matter.

In our LDA approach the latter is simulated by considering the $N = Z = A/2$ nucleus, but we analyze two possibilities. First, on the basis of Eqs. (1) and (2) with $e = \mathcal{E}(r)/\rho$, we present the integrand of the right-hand side of the following expression for $I^2 e_{\text{sym}}(A, T)$ as a difference of two terms with transparent physical meaning:

$$I^2 e_{\text{sym}}(A, T) = \int d\vec{r} \left[\frac{\mathcal{E}(\rho_A(r), \delta, T)}{A} - \frac{\mathcal{E}(\rho_{A_1}(r), \delta = 0, T)}{A_1} \right], \quad (18)$$

in which the first one corresponds to the energy per volume and particle of nuclear matter $\mathcal{E}(\rho_A(r), \delta, T)/A$ with a density $\rho_A(r)$ equal to that of the considered nucleus with A nucleons, Z protons, and N neutrons from the given isotopic chain. The second term $\mathcal{E}(\rho_{A_1}(r), \delta = 0, T)/A_1$ is analogous for the isotope with $A_1 = 2Z$ ($N_1 = Z = A_1/2$). For example, for the Ni isotopic chain the nucleus A_1 is the double-closed shell nucleus ^{56}Ni ($Z = N_1 = 28$), while for the Sn isotopic chain the nucleus A_1 is the double-closed shell nucleus ^{100}Sn ($Z = N_1 = 50$) and both ^{56}Ni and ^{100}Sn isotopes play a role of reference nuclei.

Our second new definition of $e_{\text{sym}}(A, T)$ is based on the expression (16) that is for finite nuclei. The latter allows us, using the LDA, to present $e_{\text{sym}}(A, T)$ in the form

$$I^2 e_{\text{sym}}(A, T) = \int \frac{d\vec{r}}{A} [\mathcal{E}(\rho_A(r), \delta, T) - \mathcal{E}(\rho_{\bar{A}}(r), N = \bar{A}/2, Z = \bar{A}/2, \delta = 0, T)], \quad (19)$$

in which the mass number $\bar{A} = A$ is the same, but with different nucleon content, $A(Z, N)$ and $\bar{A}(Z = \bar{A}/2, N = \bar{A}/2)$. This consideration requires the even-even nucleus with $N = Z = \bar{A}/2$ to be bound.

In the calculations (with results presented in Sec. III B), the T -dependent densities and kinetic energy densities are calculated by using Eqs. (1)–(4), as well as the HFBTHO code. For a comparison, the results obtained by using TF expression with T^2 term for the T -dependent kinetic energy densities [Eq. (9)], as well as those obtained by using T -dependent densities from the ETF method [Eq. (14)] and the RDFA [Eq. (15)] for ^{208}Pb nucleus, are also presented in Sec. III B.

III. RESULTS FOR Ni, Sn, AND Pb ISOTOPIC CHAINS AND DISCUSSION

A. Temperature-dependent densities, nuclear radii, and neutron skins

We start our analysis by studying the local density distributions $\rho(r)$ and their changes with respect to the temperature. The results for these densities of the nucleus ^{208}Pb obtained within the ETF method [Eq. (14)] and RDFA [Eq. (15)], as well as the Skyrme HFB method, are given in Figs. 1 and 2, respectively. In addition to the proton and neutron densities, normalized to $Z = 82$ and $N = 126$, respectively, that are presented in the left panel of Fig. 1, we give also in the right panel of the same figure the total local density of ^{208}Pb normalized to $A = 208$. It can be seen that ETF method and RDFA yield densities that have smooth behavior with r at any temperature T although the RDFA, in contrast to the ETF

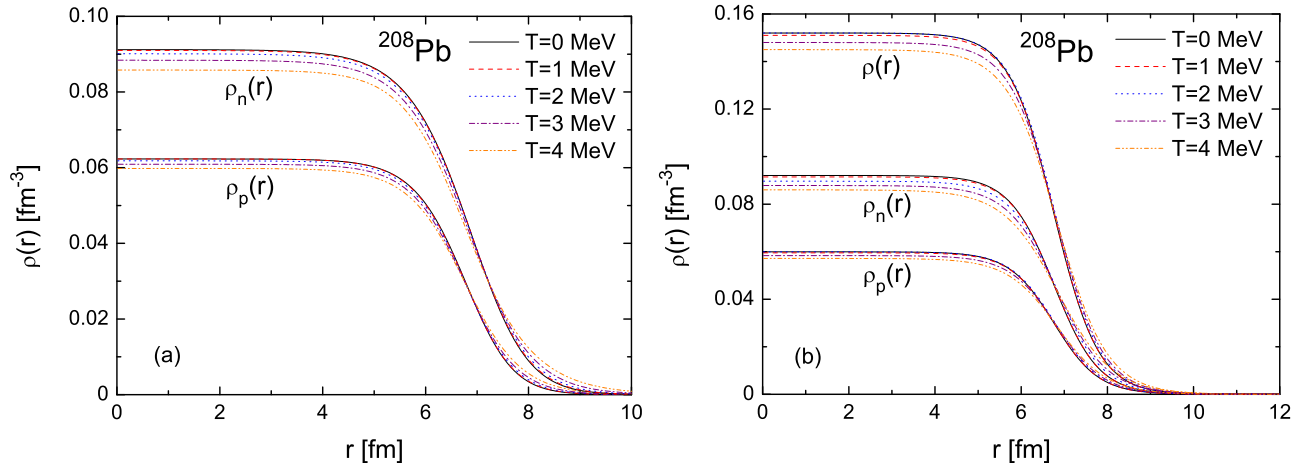


FIG. 1. Proton $\rho_p(r)$ and neutron $\rho_n(r)$ local density distributions of ^{208}Pb obtained within the ETF method (a) and R DFA (b) for temperatures $T = 0$ MeV (black solid line), $T = 1$ MeV (red dashed line), $T = 2$ MeV (blue dotted line), $T = 3$ MeV (purple dash-dotted line), and $T = 4$ MeV (yellow dash-double-dotted line). The total density distribution $\rho(r)$ of ^{208}Pb obtained within the R DFA is also presented.

method, incorporates the THF shell effects [76]. Figure 1 also shows that with increasing temperature all type of densities decrease in the central part of the nucleus. This decrease is stronger for the neutron distributions of ^{208}Pb . The proton and neutron local density distributions of ^{208}Pb obtained within the Skyrme HFB method in Fig. 2 have somewhat different behavior. The same trend with the increase of the temperature can be observed, but in this case the HFBTHO densities exhibit a stronger T dependence. At the same time, it is observed that the nuclear surface becomes more diffuse with increasing T , while a similar reduction of the densities at the center of the nucleus shown in Fig. 1 takes place. This is a natural consequence of the weakness of the shell effects with increasing T .

In Fig. 3 we display as examples the density distributions of protons and neutrons for double-magic ^{78}Ni and ^{132}Sn nuclei at $T = 0, 2,$ and 4 MeV obtained by using the SLy4 and SkM* parametrizations within the HFB method. It can be seen from Fig. 3 that the differences between the curves

corresponding to the three temperatures are smaller in these nuclei in comparison with the case of ^{208}Pb shown in Fig. 2. The tendency in the behavior of proton and neutron densities of ^{78}Ni and ^{132}Sn obtained with a given Skyrme force (SLy4 or SkM*) is similar. For example, the use of both parametrizations leads to a depression of the proton densities in the interior of ^{132}Sn [Figs. 3(c) and 3(d)] being larger at zero temperature and to a growth in the same region for the neutron densities, but in an opposite direction relative to T [Figs. 3(c') and 3(d')]. As a consequence, a spatial extension of both densities at the surface region is observed with the increase of T . Namely this region is responsible for the emergence of a neutron skin (e.g., Ref. [38]).

We show in Figs. 4–6 the neutron and proton rms radii [Eq. (12)] and their difference, known as the neutron-skin thickness [Eq. (13)], as a function of the mass number A for Ni ($A = 60$ – 82), Sn ($A = 124$ – 152), and Pb ($A = 202$ – 214) isotopic chains, respectively, calculated by using SLy4 force.

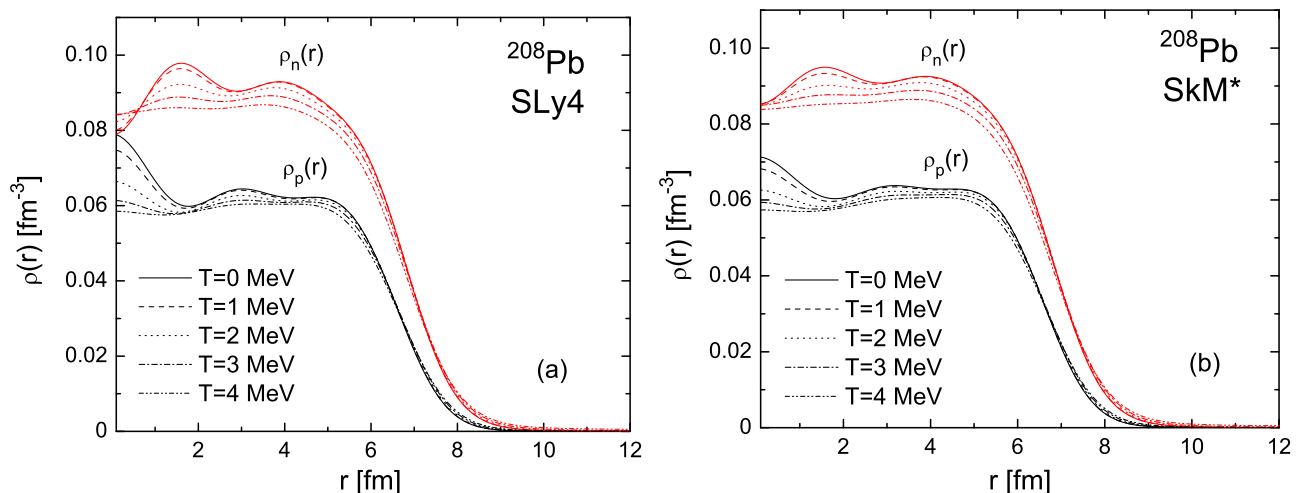


FIG. 2. Proton and neutron local density distributions of ^{208}Pb obtained within the HFBTHO method [71] with SLy4 (a) and SkM* (b) forces. Five different curves for protons (in black) and neutrons (in red) represent the results for the corresponding densities for temperatures $T = 0$ (solid line), $T = 1$ MeV (dashed line), $T = 2$ MeV (dotted line), $T = 3$ MeV (dash-dotted line), and $T = 4$ MeV (dash-double-dotted line).

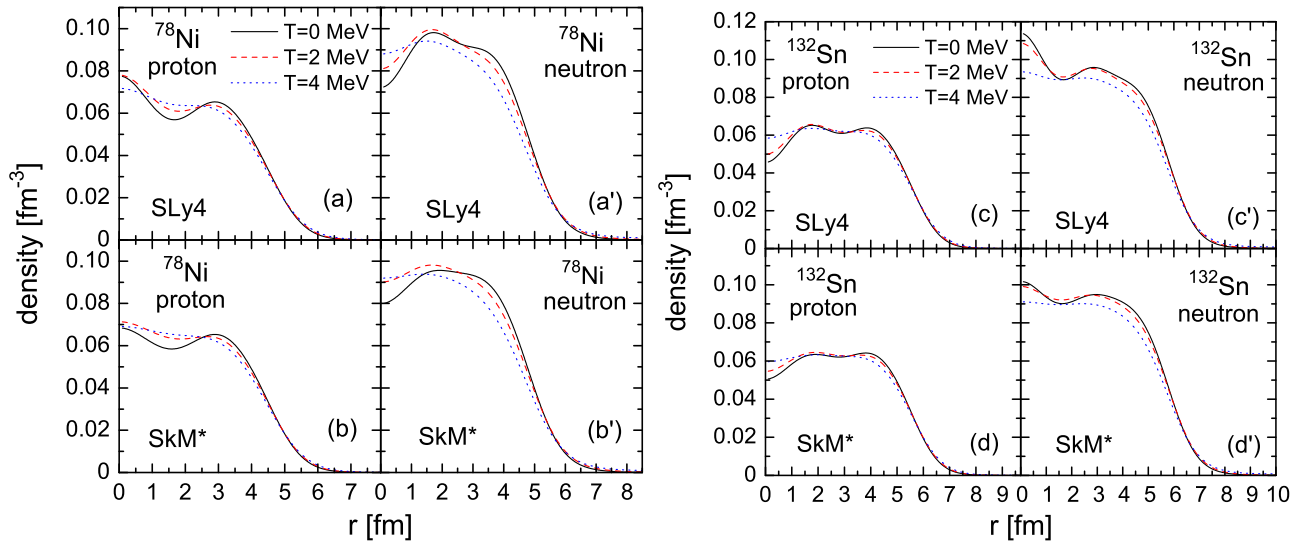


FIG. 3. HFBTHO density distributions of protons and neutrons for ^{78}Ni [(a), (a'), (b), (b')] and ^{132}Sn [(c), (c'), (d), (d')] at $T = 0$ MeV (solid line), $T = 2$ MeV (dashed line), and $T = 4$ MeV (dotted line) obtained using the SLy4 and SkM* parametrizations.

First, it can be seen that the proton rms radii for all cases increase more slowly than the neutron ones, which is valid for all the isotopic chains and temperatures. This is naturally expected in isotopic chains where the number of protons remains fixed. In addition, while the results of both radii at $T = 0$ and $T = 2$ MeV are close to each other with increasing A , one can see a steep increase of their values when the nucleus become very hot ($T = 4$ MeV). In the case of Pb isotopes there is almost no change of the proton radius within the chain at $T = 4$ MeV [Fig. 6(a)]. The neutron rms radii for the same chain tend to increase [see Fig. 6(b)], but not so rapidly as they increase for the Ni and Sn isotopes (Figs. 4 and 5). As can be seen from Figs. 4(c), 5(c), and 6(c), the neutron-skin thickness exhibits the same trend as the rms radii. It grows significantly with the increase of T , being much larger at $T = 4$ MeV than at lower temperatures $T = 0, 2$ MeV.

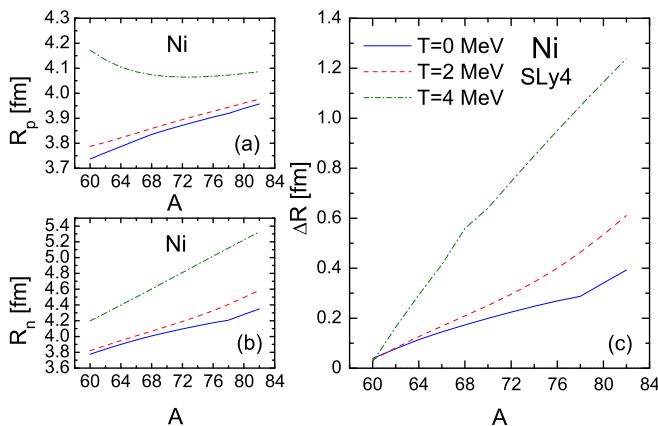


FIG. 4. Mass dependence of the proton R_p (a) and neutron R_n (b) radius of the Ni isotopes ($A = 60$ – 82) calculated with the SLy4 interaction at $T = 0$ MeV (solid line), $T = 2$ MeV (dashed line), and $T = 4$ MeV (dash-dotted line). Neutron skin thickness ΔR as a function of A (c) for the Ni isotopes.

The mechanism of formation of neutron skin in tin isotopes has been studied in Ref. [37], where the changes in the neutron skin was attributed mainly to the effect of temperature on the occupation probabilities of the single-particle states around the Fermi level. In [37] a more limited Sn isotopic chain up to ^{120}Sn was considered. Our results for larger A in this chain (from $A = 124$ to $A = 152$) also show a slow increase of the neutron skin size. The enhancement of the proton and neutron radii at high temperatures leads to a rapid increase of the neutron skin size. We would like to note that at zero temperature the use of HFBTHO temperature-dependent densities in the present approach confirms the observation in our previous work [38] (where the densities were calculated within a deformed Skyrme HF+BCS approach), namely that a pronounced neutron skin can be expected at $A > 132$ in Sn and $A > 74$ in Ni isotopes.

The results for the proton and neutron radii and their difference (neutron-skin thickness) as a function of the temperature T for selected ^{60}Ni , ^{78}Ni , and ^{82}Ni isotopes, are illustrated in Fig. 7. The calculations are made by using the

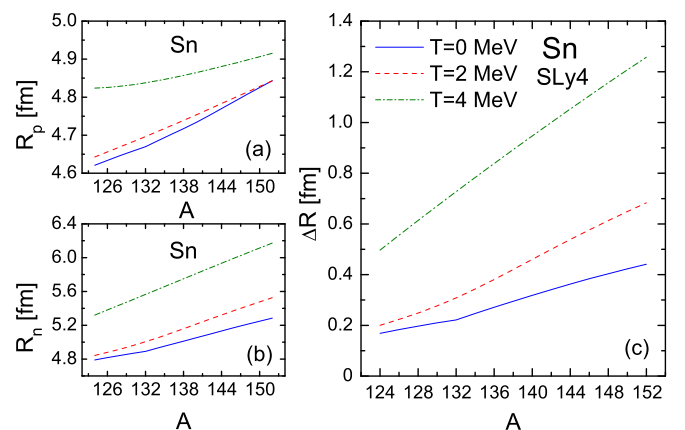


FIG. 5. Same as in Fig. 4, but for Sn isotopes ($A = 124$ – 152).

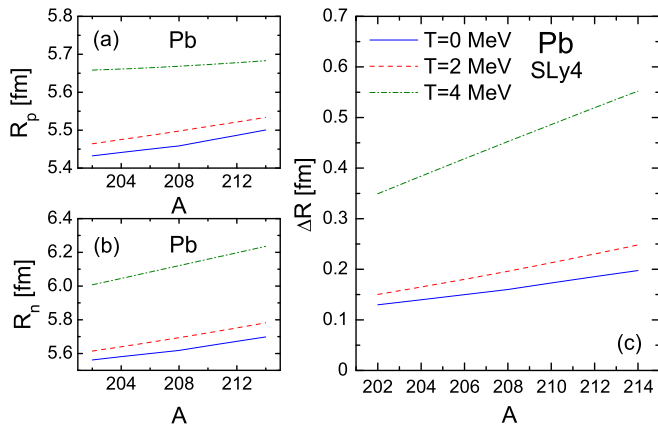


FIG. 6. Same as in Fig. 4, but for Pb isotopes ($A = 200$ – 214).

SLy4 parametrization. In addition, similar plots with results for three tin (^{124}Sn , ^{132}Sn , ^{152}Sn) and lead (^{202}Pb , ^{208}Pb , ^{214}Pb) isotopes are presented in Figs. 8 and 9, respectively. In the temperature range $T = 0$ – 4 MeV considered in the present work, we find a very slow increase of the proton radius compared to the rapid increase of the neutron radius with the temperature. As seen from Fig. 7(a), only for the ^{60}Ni nucleus both proton and neutron rms radii are very similar and behave similarly with temperature. In fact, the dependence of the neutron skin thickness with temperature in ^{60}Ni is very small and we observe only a tiny effect compatible with an almost null skin thickness [we note the small scale in ^{60}Ni in Fig. 7(a')] in comparison with those of ^{78}Ni and ^{82}Ni in Figs. 7(b') and

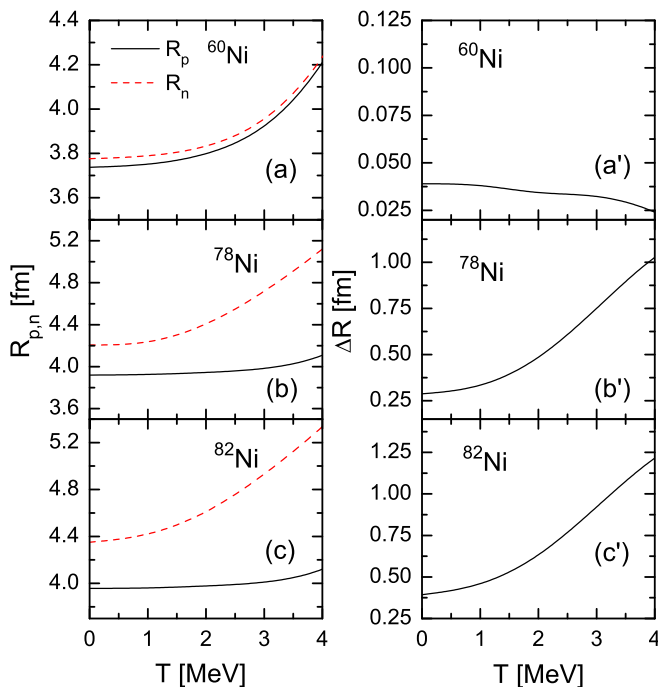


FIG. 7. Left: Proton R_p (solid line) and neutron R_n (dashed line) radius of ^{60}Ni , ^{78}Ni , and ^{82}Ni isotopes with respect to the temperature T calculated with SLy4 interaction. Right: Neutron skin thickness ΔR for the same Ni isotopes as a function of T .

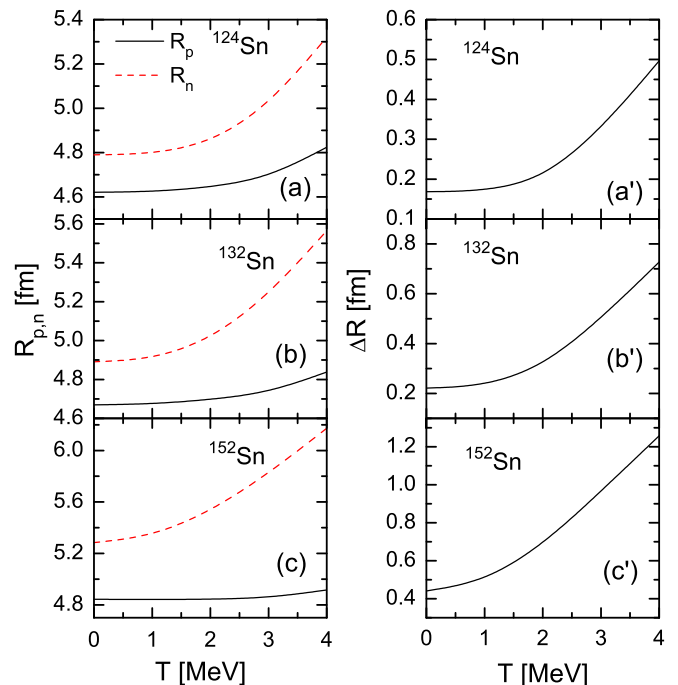


FIG. 8. Same as in Fig. 7, but for ^{124}Sn , ^{132}Sn , and ^{152}Sn isotopes.

7(c'), respectively]. Here we would like to note that the use of the SkM* interaction leads to results for the proton and neutron radii, as well as for the neutron skin thickness of the considered isotopes, very similar to those obtained by using of SLy4 Skyrme force and presented in Figs. 4–9.

The temperature dependence of rms radii obtained in this work for ^{208}Pb can be compared to that shown in Ref. [21].

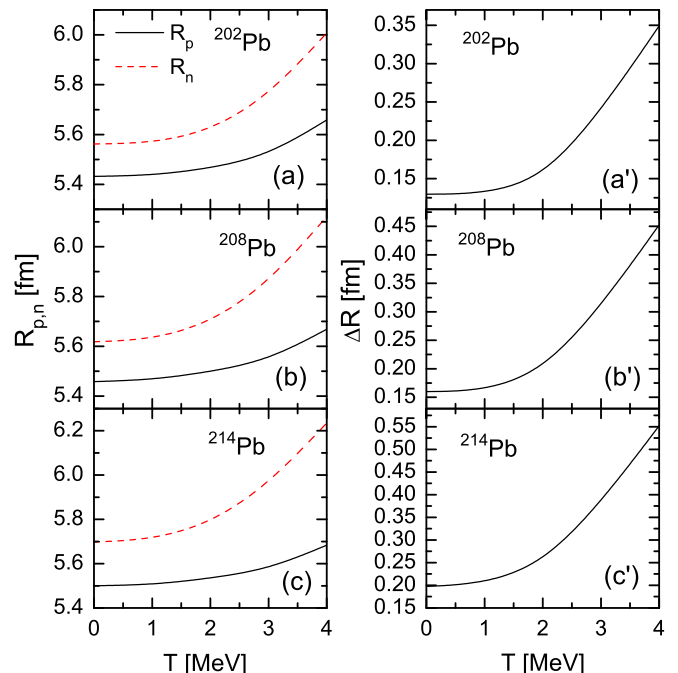


FIG. 9. Same as in Fig. 7, but for ^{202}Pb , ^{208}Pb , and ^{214}Pb isotopes.

In the latter work properties of hot nuclei have been studied within the relativistic TF approximation and different RMF parametrizations were tested. The temperature dependence of the proton radius agrees well with that of Ref. [21], which in the range below $T = 4$ MeV is quite independent of the RMF parametrization used. On the other hand, the temperature dependence of the neutron radius in [21] is more sensitive to the RMF parametrization used. The dependence on T of the neutron radii in our calculations is more pronounced, increasing with T much faster than those in Ref. [21]. As a result, the neutron skin thickness, which is rather flat in [21], increases more rapidly with T in our calculations. It

turns out that we get values of the neutron skin thickness at zero temperature (0.16 fm) similar to those obtained in [21] by using the FSU parametrization. As pointed out in Ref. [38], the RMF results for ΔR systematically overestimate the Skyrme HF results. This is confirmed by the larger values of the neutron-skin thickness of ^{208}Pb obtained in Ref. [21] when using NL3 and TM1 models.

B. Temperature dependence of the symmetry energy coefficient

In understanding the symmetry energy coefficient e_{sym} for finite nuclear systems and their thermal evolution, some ambiguities about their proper definition could be noted. First, we use the new definition of the symmetry energy coefficient e_{sym} given by Eq. (18), and the results for several nuclei from the three isotopic chains calculated with SkM* interaction are presented in Fig. 10. They are obtained by simultaneous consistent treatment of both T -dependent nucleon densities and kinetic energy densities within the HFB method and computed by the HFBTHO code. As noted in Sec. II D, there exist difficulties in the calculations of the term $e(\rho, \delta = 0, T)$ of Eq. (2) for symmetric nuclear matter; namely, of using the reference case $\delta = 0$ when the nucleus with $Z = N_1$ is unbound. Keeping this in mind, as an attempt, for Ni and Sn isotopes we take as reference nuclei (A_1) the nuclei ^{56}Ni ($Z = N_1 = 28$) and ^{100}Sn ($Z = N_1 = 50$), respectively. The case of the Pb isotopic chain is even more difficult because the eventual nucleus of reference with $Z = N_1 = 82$ is clearly unbound and there do not exist appropriate bound nuclei for the purpose. As a way to overcome this difficulty, we try in this case to use again the ^{100}Sn as a reference nucleus with $Z = N_1 = 50$, normalized with $A_1 = 100$ in Eq. (18).

The symmetry energy coefficient exhibits almost flat behavior for the double-magic ^{78}Ni and ^{132}Sn nuclei. Here we would like also to emphasize that if one extends the temperature range, the values of e_{sym} may become negative.

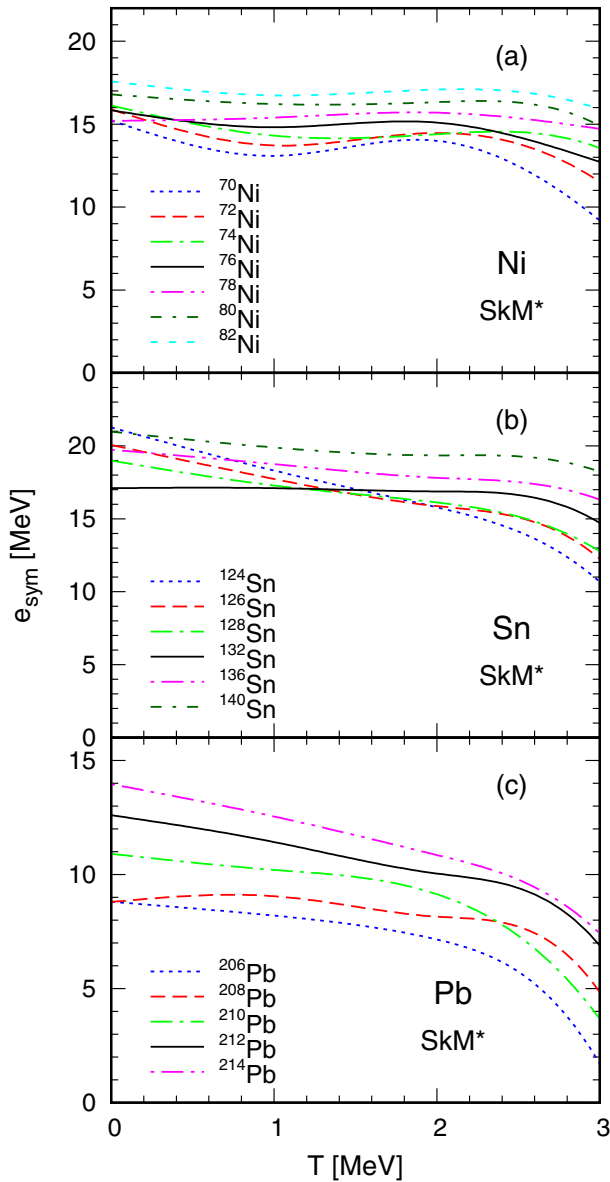


FIG. 10. Temperature dependence of the symmetry energy coefficient e_{sym} obtained by using Eq. (18) for several nuclei from Ni ($A = 70$ – 82) (a), Sn ($A = 124$ – 140) (b), and Pb ($A = 206$ – 214) (c) isotopic chains with SkM* force. The nucleon densities and kinetic energy densities used to calculate e_{sym} are consistently derived from HFBTHO code.

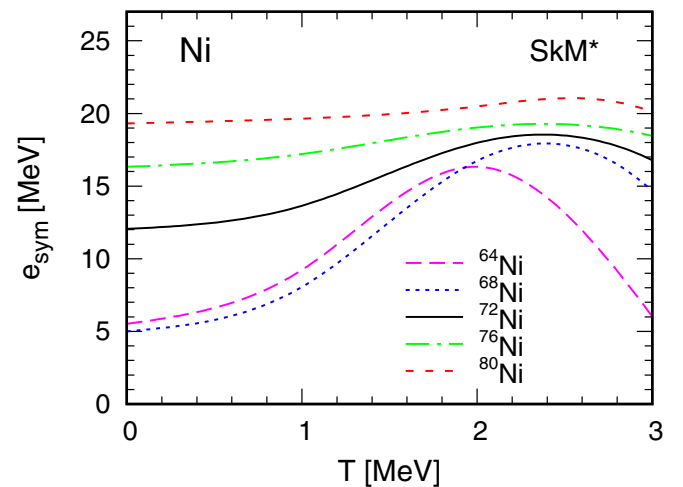


FIG. 11. Temperature dependence of the symmetry energy coefficient e_{sym} obtained by using Eq. (19) for several nuclei from Ni ($A = 64$ – 80) isotopic chain with the SkM* force. The nucleon densities and kinetic energy densities used to calculate e_{sym} are consistently derived from HFBTHO code.

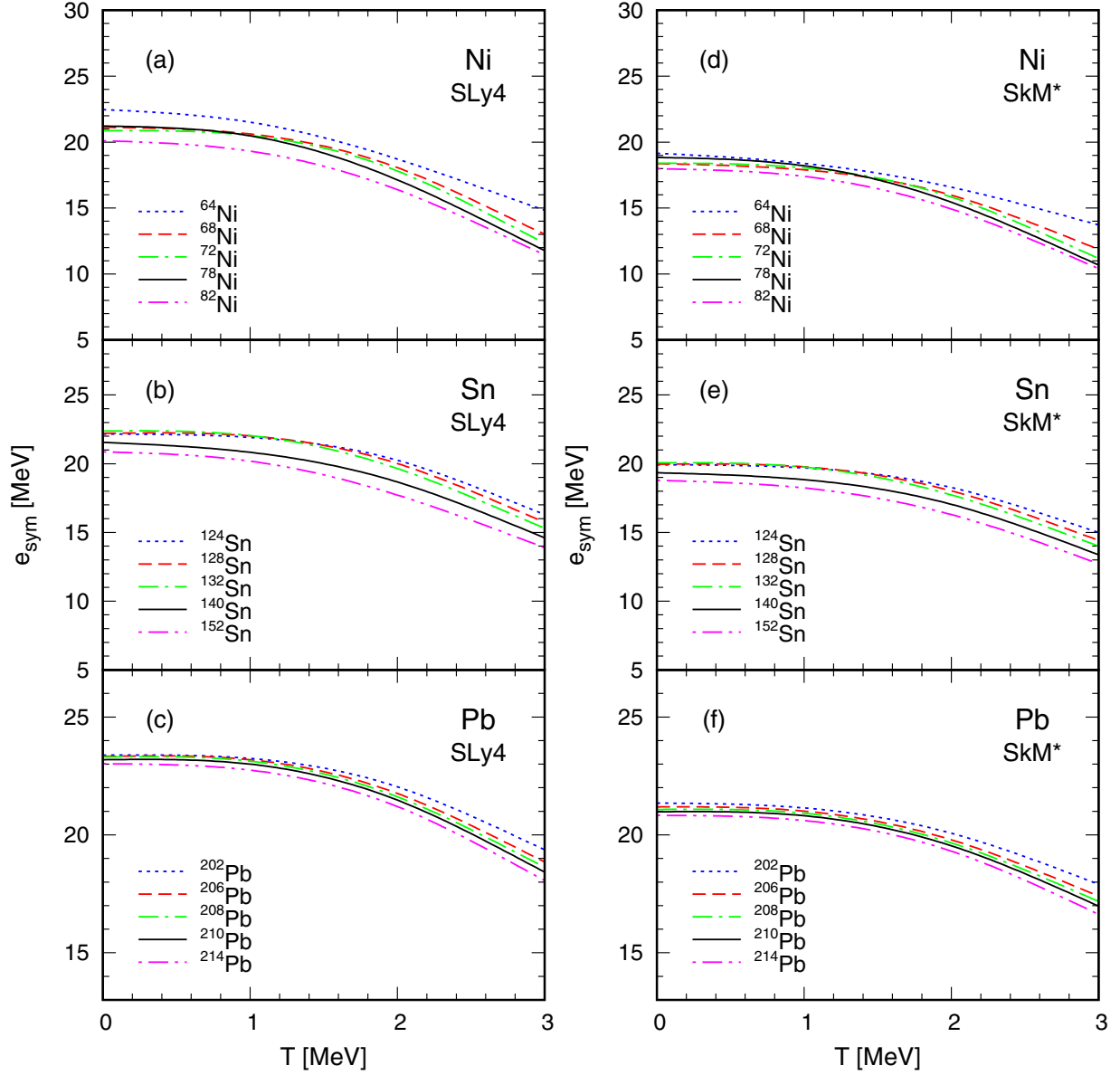


FIG. 12. Temperature dependence of the symmetry energy coefficient e_{sym} obtained for several nuclei from Ni ($A = 64$ – 82) [(a) and (d)], Sn ($A = 124$ – 152) [(b) and (e)], and Pb ($A = 202$ – 214) [(c) and (f)] isotopic chains in HFB method with SLy4 (left panel) and SkM* (right panel) forces. The results of e_{sym} are obtained by using Eqs. (1)–(4) with HFBTHO densities and T^2 approximation for the kinetic energy density [Eq. (9)].

This fact has been already discussed in the literature, for instance in Refs. [7,21], where a subtraction procedure has been employed for modeling the hot nucleus. The negativity of e_{sym} at high temperatures violates the general understanding of the symmetry energy. Generally, however, in our opinion the expression (18) is reliable, particularly when considering isotopic chains, but obviously the question about the proper definition of the symmetry energy coefficients for finite nuclei still remains open.

As a next step of our work, we give in Fig. 11 the results for the symmetry energy coefficient of five Ni isotopes obtained by using Eq. (19) and SkM* force. The same difficulties noted above at the discussion of the results presented in Fig. 10 and obtained by using Eq. (18), appear in this case. We limited

ourselves to these cases because, as mentioned in Sec. II D, the even-even nucleus with $N = Z = \bar{A}/2$ ($\bar{A} = A$) should be bound. This is possible only for Ni isotopes but not for Sn and Pb ones. For instance, in the case of Sn isotopes all the $N = Z$ nuclei with \bar{A} ($\bar{A} = A$) starting at 124 ($N = Z = 62$) are unbound. So, we consider the cases ^{64}Ni : $N = Z = 32$ (^{64}Ge), ^{68}Ni : $N = Z = 34$ (^{68}Se), ^{72}Ni : $N = Z = 36$ (^{72}Kr), ^{76}Ni : $N = Z = 38$ (^{76}Kr), ^{80}Ni : $N = Z = 40$ (^{80}Zr). In contrast to the results presented in Fig. 10 and further in Fig. 12, the $e_{\text{sym}}(A, T)$ for the Ni isotopes calculated using Eq. (19) and shown in Fig. 11 do not decrease smoothly and have a different behavior. As already mentioned above, the question of calculating the symmetry energy coefficient for heavy nuclei with a large isospin asymmetry needs more effort in order

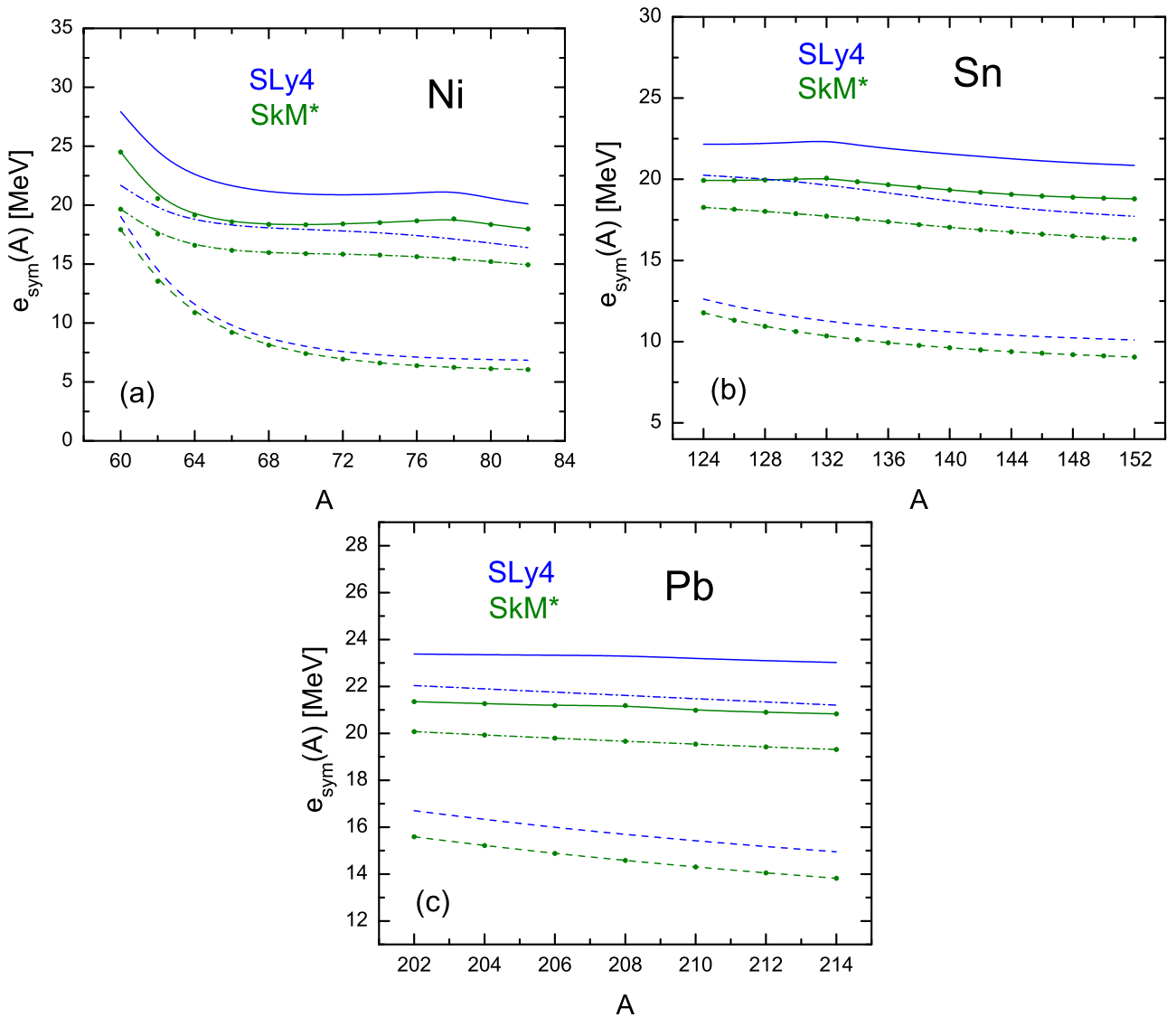


FIG. 13. The mass dependence of the symmetry energy coefficient e_{sym} for Ni (a), Sn (b), and Pb (c) isotopic chains at temperatures $T = 0$ MeV (solid line), $T = 2$ MeV (dash-dotted line), and $T = 4$ MeV (dashed line) calculated with SLy4 (blue lines) and SkM* (green lines with points) Skyrme interactions. The results of e_{sym} are obtained by using Eqs. (1)–(4) with HFBTHO densities and T^2 approximation for the kinetic energy density [Eq. (9)].

to overcome the ambiguities of the results for $e_{\text{sym}}(A, T)$ in finite nuclei using various definitions. In our work we suggested and used two possible ways to solve the problem. The quite different results obtained in both cases show the strong dependence of the symmetry energy coefficient for finite nuclei on the proper definition.

For completeness, we perform a comparative analysis of e_{sym} for several isotopes from the same Ni, Sn, and Pb chains applying the LDA in a version based on Eqs. (1)–(4). The symmetric nuclear matter part of Eq. (2) $e(\rho, \delta = 0, T)$ is obtained approximately with densities $\rho_n = \rho_p = \rho/2$, where ρ is the total density calculated with the HFBTHO code. The kinetic energy density is from the TF method with the T^2 term [22] in Eq. (9) calculated with the above densities. So, in this case $\tau_n \approx \tau_p$. The results are presented in Figs. 12 and 13. Figure 12 illustrates the isotopic evolution of the symmetry

energy coefficient on the examples of Ni ($A = 64$ –82), Sn ($A = 124$ –152), and Pb ($A = 202$ –214) chains in the case of both SLy4 and SkM* Skyrme interactions used in the calculations. A smooth decrease of e_{sym} is observed with the increase of the mass number. Unfortunately, it is difficult to compare our results with other theoretical calculations of e_{sym} of nuclei from the mass range covered in the present work except from the results for ^{208}Pb shown in Refs. [4, 21] and for the mass number $A = 120$ presented in Fig. 5 of Ref. [7]. The mass dependence of $e_{\text{sym}}(A)$ calculated by using the same roadmap [Eqs. (1)–(9)] and densities from the HFBTHO code is displayed in Fig. 13 for Ni, Sn, and Pb isotopic chains for the same SLy4 and SkM* interactions at three temperatures, $T = 0, 2$, and 4 MeV. On one hand, one can see that the values of e_{sym} calculated with SLy4 overestimate those obtained with the SkM* force. From another viewpoint,

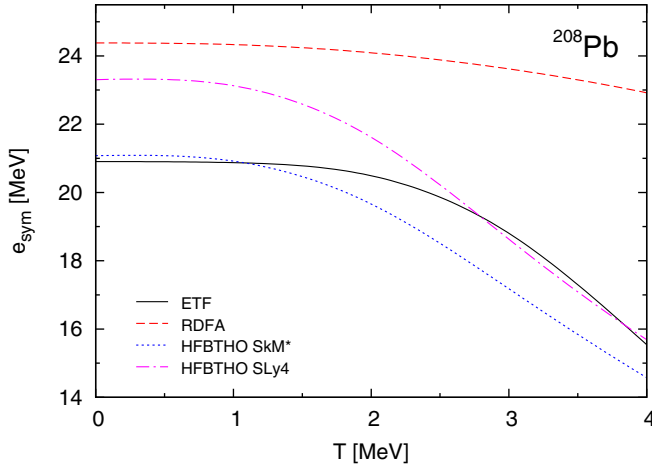


FIG. 14. Comparison of the results for the symmetry energy coefficient e_{sym} for ^{208}Pb calculated with ETF [Eq. (14)], RDFA [Eq. (15)], and HFB (with SkM* and SLy4 forces) densities. They are obtained by using Eqs. (1)–(4) and T^2 approximation for the kinetic energy density [Eq. (9)].

the difference between both sets of values decreases when going to higher temperatures, in such a way that it is small at the transition from $T = 0$ to $T = 2$ MeV and a “gap” appears between the results corresponding to $T = 2$ and $T = 4$ MeV. For the Pb isotopic chain even a “crossover” of curves that correspond to temperatures $T = 0$ and $T = 2$ MeV and both parametrizations is observed in Fig. 13(c). We also would like to note the existence of a kink in the values of $e_{\text{sym}}(A)$ at zero temperature at the double-magic ^{78}Ni and ^{132}Sn nuclei [see Figs. 13(a) and 13(b)] as well as the lack of kinks in the Pb isotopic chain [Fig. 13(c)]. These results confirm our previous observations when studying the density dependence of the symmetry energy for Ni, Sn, and Pb isotopes [8,9]. We also note that in the cases of $e_{\text{sym}}(A)$ for Ni and Sn isotopic chains the kinks exist for $T = 0$ MeV, but not for $T = 2$ and $T = 4$ MeV. The reason is the well-known fact that the shell effects can be expected up to $T \leq 2$ MeV. One can see that the values of e_{sym} of isotopes in the three chains at $T = 0$ MeV obtained by following this procedure are larger than those shown in Fig. 10 obtained by using Eq. (18) with densities and kinetic energy densities obtained consistently using the HFBTHO code. This can be due to the not realistic choice of the reference nucleus in the Pb chain (^{100}Sn) within the previous procedure [Eq. (18)].

As a next step we present in Fig. 14 the results for ^{208}Pb obtained using Eqs. (1)–(9) with three different densities, namely those obtained within the ETF, RDFA, and HFB (with SkM* and SLy4 forces) methods. The kinetic energy densities are obtained within TF method with T^2 term [Eq. (9)]. The results for the thermal evolution of the symmetry energy coefficient in the interval $T = 0$ –4 MeV show that its values decrease with temperature being larger in the case of symmetrized-Fermi density of ^{208}Pb obtained within the RDFA. As already discussed, the applications of different methods fail to give unique values for the symmetry energies for finite nuclei or their temperature dependence. Nevertheless,

we would like to note that our results for e_{sym} are close to the result obtained within the LDA (in a version reported in Ref. [4]) and within the relativistic TF approximation in Ref. [21] for the same nucleus. The differences in the results can be referred to the different calculation ingredients (nucleon densities, kinetic energy density, etc.) or the adopted procedure to obtain the symmetry energy coefficient.

IV. CONCLUSIONS

In this work, a theoretical approach to the nuclear many-body problem has been used to study the temperature dependence of the symmetry energy coefficient in finite nuclei and other properties, such as the T -dependent nucleon densities and related rms radii, as well as the possibility of formation of neutron skins. The approach uses as a ground previous considerations within the local-density approximation (e.g., Refs. [4–7]) combining it with the self-consistent Skyrme-HFB method using the cylindrical transformed deformed harmonic oscillator basis [71,72]. For infinite nuclear matter a Skyrme energy density functional with SkM* and SLy4 parametrizations is used. In our work we consider the isotopic chains of neutron-rich Ni, Sn, and Pb isotopes that represent an interest in future measurements with radioactive exotic beams. In addition to the HFBTHO densities of these isotopes, two other temperature-dependent densities of ^{208}Pb were used in the present paper: the local densities within the ETF method [29,33] that reproduce the averaged THF results up to temperature $T = 4$ MeV, and the symmetrized-Fermi local density distribution determined within the RDFA [73]. The properties of hot nuclei were modelled in a temperature range $T = 0$ –4 MeV. We have found that the ETF and RDFA results for the density distributions demonstrate a smooth function with r at any temperature T , while the Skyrme HFB densities have a stronger T dependence. In general, the density distributions decrease with the temperature in the center of the nucleus. Following the trend of the corresponding proton and neutron rms radii, the neutron-skin thickness grows significantly with the increase of T within a given isotopic chain. The calculated neutron-skin thicknesses by using HFBTHO densities show similar results when both SLy4 and SkM* interactions are used. Second, we find that at zero temperature a formation of a neutron skin can be expected to start at $A > 78$ and $A > 132$ for Ni and Sn isotopes, respectively, thus confirming our previously obtained results in Refs. [8,38].

Our investigations of the T -dependent symmetry coefficients $e_{\text{sym}}(A, T)$ for finite nuclei (in particular, cases of Ni, Sn, and Pb isotopic chains) within the LDA with some modifications face the problem of the choice of density distributions and the kinetic energy densities. In our work both quantities are calculated through the HFBTHO code that solves the nuclear Skyrme-Hartree-Fock-Bogolyubov problem by using the cylindrical transformed deformed harmonic-oscillator basis [72]. We have explored the LDA expression [Eq. (1)] for the symmetry energy $e_{\text{sym}}(A, T)$, as well as Eq. (2), the Skyrme energy density functional $\mathcal{E}(r, T)$ [the first three lines of Eq. (3)] and the nucleon effective mass [Eq. (4)]. Aiming to study the T dependence of e_{sym} within a given isotopic chain, we introduced two new definitions of $e_{\text{sym}}(A, T)$

[Eqs. (18) and (19)] within the LDA, as an attempt to analyze in a more appropriate way the symmetry energy coefficient of finite nuclei within a given chain. Particularly, for the cases when there is no $Z = N = A/2$ bound nucleus HFB solution, none of the recipes used seems to be totally justified or free from ambiguities, so that more work along this line is required. It is demonstrated that, using Eq. (18), the thermal sensitivity of the symmetry energy coefficient (Fig. 10) is comparatively weaker than the one revealed when using the procedure based on Eqs. (1)–(9). In general, the results of e_{sym} calculated for various isotopes in the present work are in good agreement with theoretical predictions for some specific nuclei reported by other authors. At the same time, however, the difference between the results given for example, in Figs. 10(a) and 11 [obtained using Eqs. (18) and (19), respectively] points out the dependence of the calculations of $e_{\text{sym}}(A, T)$ on various definitions of this quantity.

Additionally, we perform a comparative analysis of e_{sym} using the procedure given by Eqs. (1)–(4), in which the kinetic energy densities are obtained from the extension of the TF method up to T^2 term [22] [Eq. (9)] and with HFBTHO densities. The results for the thermal evolution of the symmetry energy coefficient of all isotopes obtained by the procedure (1)–(9) show that its values decrease with temperature (Fig. 12). This is observed also in the particular case of the ^{208}Pb nucleus, for which different densities have been tested to get e_{sym} . It is found from the comparison (see Fig. 14) that the use of symmetrized Fermi density obtained within the RDFA [Eq. (15)] leads to larger values of the symmetry energy coefficient. At the same time, for all isotopic chains considered and for both Skyrme forces used in the calculations, the symmetry energy coefficient decreases smoothly with the increase of the mass number in the same temperature interval (Fig. 12). In addition,

it comes out that SLy4 force produces larger values of e_{sym} than the SkM* force with a fast decrease of e_{sym} when T increases. Studying the mass dependence of the symmetry energy coefficient (Fig. 13), we would like to note also the existence of a kink in Ni and Sn isotopic chains at the double-magic ^{78}Ni and ^{132}Sn nuclei at $T = 0$ MeV, respectively, and a lack of a kink in the Pb chain. This observation confirms the result obtained previously in our works [8,9] when studying the nuclear symmetry energy of spherical neutron-rich nuclei, particularly its isotopic evolution. We pointed out that the values of e_{sym} at $T = 0$ MeV obtained within this procedure for the considered three chains are larger than those obtained by using Eq. (18) (Fig. 10) with densities and kinetic energy densities from the HFBTHO code. For Pb isotopes the values of e_{sym} are larger than those for Ni and Sn chains.

Having in mind the dependence of $e_{\text{sym}}(A, T)$ on its various definitions, we note that more refined future investigations, for instance, of the temperature dependence of both volume and surface components of the symmetry energy coefficient [7], would provide better description of hot nuclei and could minimize the ambiguities due to the use of different definitions for the symmetry energy coefficient of finite nuclei. These studies based on our previous work [53] and the present one are in progress.

ACKNOWLEDGMENTS

Three of the authors (M.K.G., A.N.A., and D.N.K) are grateful for support of the Bulgarian Science Fund under Contract No. DFNI-T02/19. D.N.K. is thankful for the partial support from Contract No. DFNI-E02/6 of the Bulgarian Science Fund. E.M.G. and P.S. acknowledge support from MINECO (Spain) under Contract No. FIS2014–51971–P.

-
- [1] J. M. Lattimer and M. Prakash, *Phys. Rep.* **442**, 109 (2007).
 [2] B. A. Li *et al.*, *Phys. Rep.* **464**, 113 (2008).
 [3] *Topical issue on Nuclear Symmetry Energy*, edited by B.-A. Li, A. Ramos, G. Verde, and I. Vidaña, *Eur. Phys. J. A* **50**, 2 (2014).
 [4] B. K. Agrawal, J. N. De, S. K. Samaddar, M. Centelles, and X. Viñas, *Eur. Phys. J. A* **50**, 19 (2014).
 [5] S. K. Samaddar, J. N. De, X. Viñas, and M. Centelles, *Phys. Rev. C* **76**, 041602(R) (2007).
 [6] S. K. Samaddar, J. N. De, X. Viñas, and M. Centelles, *Phys. Rev. C* **78**, 034607 (2008).
 [7] J. N. De and S. K. Samaddar, *Phys. Rev. C* **85**, 024310 (2012).
 [8] M. K. Gaidarov, A. N. Antonov, P. Sarriguren, and E. M. de Guerra, *Phys. Rev. C* **84**, 034316 (2011).
 [9] M. K. Gaidarov, A. N. Antonov, P. Sarriguren, and E. M. de Guerra, *Phys. Rev. C* **85**, 064319 (2012).
 [10] M. K. Gaidarov, P. Sarriguren, A. N. Antonov, and E. M. de Guerra, *Phys. Rev. C* **89**, 064301 (2014).
 [11] D. V. Shetty and S. J. Yennello, *Pramana* **75**, 259 (2010).
 [12] S. Kowalski, J. B. Natowitz, S. Shlomo, R. Wada, K. Hagel, J. Wang, T. Materna, Z. Chen, Y. G. Ma, L. Qin, A. S. Botvina, D. Fabris, M. Lunardon, S. Moretto, G. Nebbia, S. Pesente, V. Rizzi, G. Viesti, M. Cinausero, G. Prete, T. Keutgen, Y. ElMasri, Z. Majka, and A. Ono, *Phys. Rev. C* **75**, 014601 (2007).
 [13] Z. H. Li, U. Lombardo, H.-J. Schulze, W. Zuo, L. W. Chen, and H. R. Ma, *Phys. Rev. C* **74**, 047304 (2006).
 [14] J. Piekarewicz and M. Centelles, *Phys. Rev. C* **79**, 054311 (2009).
 [15] I. Vidaña, C. Providência, A. Polls, and A. Rios, *Phys. Rev. C* **80**, 045806 (2009).
 [16] F. Sammarruca and P. Liu, *Phys. Rev. C* **79**, 057301 (2009).
 [17] P. Danielewicz, [arXiv:1003.4011](https://arxiv.org/abs/1003.4011) [nucl-th].
 [18] Ch. C. Moustakidis, *Phys. Rev. C* **76**, 025805 (2007).
 [19] F. Sammarruca, *J. Phys. G* **37**, 085105 (2010).
 [20] B. K. Agrawal, D. Bandyopadhyay, J. N. De, and S. K. Samaddar, *Phys. Rev. C* **89**, 044320 (2014).
 [21] Z. W. Zhang, S. S. Bao, J. N. Hu, and H. Shen, *Phys. Rev. C* **90**, 054302 (2014).
 [22] S. J. Lee and A. Z. Mekjian, *Phys. Rev. C* **82**, 064319 (2010).
 [23] Bao-An Li and Lie-Wen Chen, *Phys. Rev. C* **74**, 034610 (2006).
 [24] A. Z. Mekjian, S. J. Lee, and L. Zamick, *Phys. Rev. C* **72**, 044305 (2005).
 [25] J. Xu, L.-Wen Chen, B.-A. Li, and H.-R. Ma, *Phys. Rev. C* **75**, 014607 (2007); **77**, 014302 (2008); *Phys. Lett. B* **650**, 348 (2007).

- [26] E. Baron, J. Cooperstein, and S. Kahana, *Phys. Rev. Lett.* **55**, 126 (1985).
- [27] A. W. Steiner, *Phys. Rev. C* **77**, 035805 (2008).
- [28] M. Brack and P. Quentin, *Phys. Lett. B* **52**, 159 (1974); *Phys. Scr. A* **10**, 163 (1974).
- [29] M. Brack, C. Guet, and H. K. Håkansson, *Phys. Rep.* **123**, 276 (1985).
- [30] E. Suraud, *Nucl. Phys. A* **462**, 109 (1987).
- [31] P. Bonche, S. Levit, and D. Vautherin, *Nucl. Phys. A* **427**, 278 (1984); **436**, 265 (1985).
- [32] J. N. De, N. Rudra, S. Pal, and S. K. Samaddar, *Phys. Rev. C* **53**, 780 (1996).
- [33] M. Brack, *Phys. Rev. Lett.* **53**, 119 (1984).
- [34] E. Khan, N. Van Giai, and N. Sandulescu, *Nucl. Phys. A* **789**, 94 (2007).
- [35] N. Sandulescu, *Phys. Rev. C* **70**, 025801 (2004).
- [36] C. Monrozeau, J. Margueron, and N. Sandulescu, *Phys. Rev. C* **75**, 065807 (2007).
- [37] E. Yüksel, E. Khan, K. Bozkurt, and G. Colò, *Eur. Phys. J. A* **50**, 160 (2014).
- [38] P. Sarriguren, M. K. Gaidarov, E. M. de Guerra, and A. N. Antonov, *Phys. Rev. C* **76**, 044322 (2007).
- [39] F. Tondeur, M. Brack, M. Farine, and J. Pearson, *Nucl. Phys. A* **420**, 297 (1984).
- [40] C. J. Horowitz and J. Piekarewicz, *Phys. Rev. Lett.* **86**, 5647 (2001); *Phys. Rev. C* **64**, 062802 (2001).
- [41] S. Typel and B. A. Brown, *Phys. Rev. C* **64**, 027302 (2001).
- [42] S. Yoshida and H. Sagawa, *Phys. Rev. C* **69**, 024318 (2004).
- [43] M. Warda, X. Viñas, X. Roca-Maza, and M. Centelles, *Phys. Rev. C* **80**, 024316 (2009).
- [44] F. J. Fattoyev and J. Piekarewicz, *Phys. Rev. C* **86**, 015802 (2012); F. J. Fattoyev, W. G. Newton, J. Xu, and B.-A. Li, *ibid.* **86**, 025804 (2012).
- [45] J. Erler, C. J. Horowitz, W. Nazarewicz, M. Rafalski, and P.-G. Reinhard, *Phys. Rev. C* **87**, 044320 (2013).
- [46] S. J. Lee and A. Z. Mekjian, *J. Korean Phys. Soc.* **62**, 1600 (2013).
- [47] B. A. Brown, *Phys. Rev. Lett.* **85**, 5296 (2000).
- [48] R. Furnstahl, *Nucl. Phys. A* **706**, 85 (2002).
- [49] P.-G. Reinhard and W. Nazarewicz, *Phys. Rev. C* **81**, 051303 (2010).
- [50] X. Roca-Maza, M. Centelles, X. Viñas, and M. Warda, *Phys. Rev. Lett.* **106**, 252501 (2011).
- [51] M. Kortelainen, J. Erler, W. Nazarewicz, N. Birge, Y. Gao, and E. Olsen, *Phys. Rev. C* **88**, 031305 (2013).
- [52] C. Mondal, B. K. Agrawal, M. Centelles, G. Colò, X. Roca-Maza, N. Paar, X. Viñas, S. K. Singh, and S. K. Patra, *Phys. Rev. C* **93**, 064303 (2016).
- [53] A. N. Antonov, M. K. Gaidarov, P. Sarriguren, and E. M. de Guerra, *Phys. Rev. C* **94**, 014319 (2016).
- [54] M. Warda, X. Viñas, X. Roca-Maza, and M. Centelles, *Phys. Rev. C* **81**, 054309 (2010).
- [55] M. Centelles, X. Roca-Maza, X. Viñas, and M. Warda, *Phys. Rev. C* **82**, 054314 (2010).
- [56] P. Danielewicz, *Nucl. Phys. A* **727**, 233 (2003).
- [57] P. Danielewicz, [arXiv:nucl-th/0411115](https://arxiv.org/abs/nucl-th/0411115).
- [58] P. Danielewicz and J. Lee, *Nucl. Phys. A* **922**, 1 (2014), and references therein.
- [59] P. Danielewicz and J. Lee, *Int. J. Mod. Phys. E* **18**, 892 (2009).
- [60] P. Danielewicz and J. Lee, *AIP Conf. Proc.* **1423**, 29 (2016).
- [61] M. B. Tsang, J. R. Stone, F. Camera, P. Danielewicz, S. Gandolfi, K. Hebeler, C. J. Horowitz, Jenny Lee, W. G. Lynch, Z. Kohley, R. Lemmon, P. Möller, T. Murakami, S. Riordan, X. Roca-Maza, F. Sammarruca, A. W. Steiner, I. Vidaña, and S. J. Yennello, *Phys. Rev. C* **86**, 015803 (2012).
- [62] M. B. Tsang, Yingxun Zhang, P. Danielewicz, M. Famiano, Zhuxia Li, W. G. Lynch, and A. W. Steiner, *Phys. Rev. Lett.* **102**, 122701 (2009); M. B. Tsang *et al.*, *Int. J. Mod. Phys. E* **19**, 1631 (2010).
- [63] A. Ono, P. Danielewicz, W. A. Friedman, W. G. Lynch, and M. B. Tsang, *Phys. Rev. C* **70**, 041604(R) (2004).
- [64] P. Danielewicz, [arXiv:nucl-th/0607030](https://arxiv.org/abs/nucl-th/0607030).
- [65] A. E. L. Dieperink and P. Van Isacker, *Eur. Phys. J. A* **32**, 11 (2007).
- [66] K. A. Brueckner, J. R. Buchler, S. Jorna, and R. J. Lombard, *Phys. Rev.* **171**, 1188 (1968).
- [67] K. A. Brueckner, J. R. Buchler, R. C. Clark, and R. J. Lombard, *Phys. Rev.* **181**, 1543 (1969).
- [68] A. N. Antonov, V. A. Nikolaev, and I. Zh. Petkov, *Bulg. J. Phys.* **6**, 151 (1979); *Z. Phys. A* **297**, 257 (1980); **304**, 239 (1982); *Nuovo Cimento A* **86**, 23 (1985); A. N. Antonov *et al.*, *ibid.* **102**, 1701 (1989); A. N. Antonov, D. N. Kadrev, and P. E. Hodgson, *Phys. Rev. C* **50**, 164 (1994).
- [69] A. N. Antonov, P. E. Hodgson, and I. Zh. Petkov, *Nucleon Momentum and Density Distributions in Nuclei* (Clarendon Press, Oxford, 1988); *Nucleon Correlations in Nuclei* (Springer-Verlag, Berlin, 1993).
- [70] D. Bandyopadhyay, C. Samanta, S. K. Samaddar, and J. N. De, *Nucl. Phys. A* **511**, 1 (1990).
- [71] M. V. Stoitsov, N. Schunck, M. Kortelainen, N. Michel, H. Nam, E. Olsen, J. Sarich, and S. Wild, *Comput. Phys. Commun.* **184**, 1592 (2013).
- [72] M. V. Stoitsov, J. Dobaczewski, W. Nazarewicz, and P. Ring, *Comput. Phys. Commun.* **167**, 43 (2005).
- [73] M. V. Stoitsov, I. Z. Petkov, and E. S. Kryachko, *C. R. Bulg. Acad. Sci.* **40**, 45 (1987); M. V. Stoitsov, *Nuovo Cimento A* **98**, 725 (1987).
- [74] J. Bartel, P. Quentin, M. Brack, C. Guet, and H.-B. Håkansson, *Nucl. Phys. A* **386**, 79 (1982); H. Krivine, J. Treiner, and O. Bohigas, *ibid.* **336**, 155 (1980).
- [75] E. Chabanat, P. Bonche, P. Haensel, J. Meyer, and R. Schaeffer, *Nucl. Phys. A* **635**, 231 (1998).
- [76] A. N. Antonov, J. Kanev, I. Z. Petkov, and M. V. Stoitsov, *Nuovo Cimento A* **101**, 525 (1989).